Determining the optimal transmembrane gas pressure for nitrigication in membrane-aerated biofilm reactors based on oxygen profile analysis

Authors: Rongchang Wang, Yanan Wang, & Zbigniew Lewandowski

The final publication is available at Springer via https://doi.org/10.1007/s00253-016-7553-1.

Wang, R., Xiao, F., Wang, Y., & Lewandowski, Z. (2016). Determining the optimal transmembrane gas pressure for nitrification in membrane-aerated biofilm reactors based on oxygen profile analysis. Applied Microbiology and Biotechnology, 100(17), 7699–7711. doi:10.1007/s00253-016-7553-1

Determining the optimal transmembrane gas pressure for nitrification in membrane-aerated biofilm reactors based on oxygen profile analysis

Rongchang Wang, Fan Xiao, Yanan Wang, Zbigniew Lewandowski

The goal of this study was to investigate the effect of transmembrane gas pressure (P_g) on the specific ammoni-um removal rate in a membrane-aerated biofilm reactor (MABR). Our experimental results show that the specific am-monium removal rate increased from 4 .98 t o 9.26 $gN\,m^{-2}\,day^{-1}$ when P_g increased from 2 to 20 kPa in an MABR with a biofilm thickness of approximately 600 μm. However, this improvement was not linear; there was a thresh-old of P_g separating the stronger and weaker effects of P_g. The ammonium removal rate was improved less significantly when P_g was over the threshold, indicating that there is an optimal threshold of P_g for maximizing ammonium removal in an MABR. The change in oxygen penetration depth (d_p) is less sensitive to P_g in the ammonia-oxidizing active layer than in the inactive layer in membrane-aerated biofilm. The loca-tion of the P_g threshold is at the same point as the thickness of the active layer on the curve of d_p versus P_g; thus, the active layer thickness and the optimal P_g can be determined on the basis of the changes in the slope of d_p to P_g.

Keywords: Membrane-aerated biofilm reactor · Oxygen penetration depth · Nitrification · Transmembrane gas pressure · Active layer

Introduction

Biofilm processes and biofilm reactors have a well-established position and a long history in biological wastewater treatment. The microorganisms active in these processes often use dis-solved gases as electron donors or acceptors in their respira-tion. For example, microorganisms use dissolved oxygen to oxidize organics and ammonium in the activated sludge pro-cess (Rosso, et al., 2011; Grady, et al., 2011), hydrogen to reduce oxidized contaminants and halogenated organics (Nerenberg et al., 2008; Zhao et al., 2014), and methane to support the co-metabolic oxidation of a wide range of organic compounds (Sun et al., 2013; Chen et al., 2014). Since the dissolved gases serve as reactants in the respiration processes, the mechanisms of gas delivery to biofilm microorganisms affect the microbial processes. Characterizing the relations between the mechanisms of gas delivery and the mechanisms of microbial processes in the most general way, the gas and the pollutants can both be delivered through the biofilm surface (a co-diffusion process) or the gas and the pollutants can be delivered from the opposite sides (a counter-diffusion process)(Cote et al., 1989; Brindle et al., 1998; Terada, et al., 2007; Wang, et al., 2009). One way of supplying these dissolved gases to biofilm microorganisms is through hollow-fiber membranes. This process is characterized as counter-diffu-sion, where the lumen of the membrane is pressurized with gas, which then diffuses through the membrane into the bio-film attached to the outer surface of the membrane while the pollutants are delivered to the biofilm from bulk liquid. When this process is used to deliver air or oxygen, the reactor is often called a membrane-aerated biofilm reactor (MABR) (Syron and Casey, 2008).

Compared to conventional bubble aeration, MABRs achieve higher gas transfer rates, require smaller tank sizes, and create significant energy savings and unique microbial

community structures that allow for the simultaneous removal of COD and nitrogen from wastewater (Brindle et al., 1998; Hwang et al., 2009; Shanahan and Semmens, 2006; Terada et al., 2003). Moreover, the elimination of bubbling prevents the stripping of volatile organic compounds (VOCs) and greenhouse gases and can also prevent foaming when surfactants are present (Syron and Casey, 2008).

When MABRs are used to remove nutrients, the precise control of oxygen delivery through the membrane, as demonstrated by Hibiya et al. (2003), allows the simultaneous nitrification and denitrification of domestic modified wastewater. Terada et al. (2006), for example, showed that nitrification rates in MABs can be controlled by manipulating transmembrane air pressure supply and reported that the ratio of the oxygen flux to the ammonia flux, J_{O2}/J_{NH4+}, was the crucial parameter for controlling nitrogen conversion in an MABR (Terada et al. 2007); control of the J_{O2}/J_{NH4+} ratio was achieved by adjusting the operational transmembrane gas pressure (P_g).

Several studies to date have been devoted to quantifying the effect of transmembrane gas pressure on gas transfer rate and the efficiency of microbial processes in biofilms. Lackner et al. (2010) demonstrated that the oxygen transfer rate (OTR) determines the success of nitrification in MABRs and that oxygen partial pressure influences OTR. Furthermore, high oxygen concentration at the biofilm base (>4 g-O m^{-3}) compromised the ability to optimize reactor operation for high nitrification efficiencies by adjusting the oxygen flux via the gas pressure. Downing and Nerenberg (2008) found that the ammonium flux and nitrite accumulation increased with increasing transmembrane operation pressure and that shortcut nitrification can effectively be controlled by manipulating dissolved oxygen (DO) at the membrane surface. The microelectrode measurements of Kumar et al. (2012) revealed that liquid flow influences oxygen transport into the biofilm and plays a major role in controlling the flux of oxygen across the biofilm/water interface, thus increasing the potential for aerobic biodegradation. However, some previous reports suggested that excessively high oxygen flux (using pure oxygen) inhibited the microbial growth on the membrane (Wilderer et al., 1995). Similarly Zhu et al. (2009) observed that a higher oxygen flux made a biofilm less stable in an MABR at a given COD loading. Thus, the effect of P_g on oxygen transfer or penetration and nitrification performance in MABR has yet to be clarified and requires further investigation.

Reports suggest that overall stratified metabolic activity of the biofilm determined by oxygen uptake rate in an MABR are dependent on P_g and the location of the active layer can be controlled by manipulation of P_g (Casey et al., 2000; Casey et al., 2004). However, besides the overall biofilm metabolic activity, the effect of P_g on local activity distributions in membrane-aerated biofilm needs to be investigated further.

Since one of the applications of MABRs is to control the rate of nitrification and, if possible, create conditions promoting simultaneous nitrification and denitrification, we designed this study to reveal the mechanistic effects of the transmembrane gas pressure. To this end, we investigated the effects of transmembrane gas pressure on the depth of oxygen penetration and the locations of ammonia-oxidizing active layer and inactive layer in a nitrifying biofilm deposited on a hollow-fiber gas-permeable membrane.

The goal of this study was to investigate the effect of transmembrane gas pressure (P_g) on nitrification in a membrane-aerated biofilm reactor (MABR). An MABR was operated at various P_g (2–20 kPa), and the corresponding ammonium removal efficiencies were compared and related to the applied gas pressure. At the same time, oxygen profiles in the biofilm were analyzed to reveal the effects of P_g on oxygen distribution and utilization in membrane-aerated biofilms. Therefore, we explored a novel approach to determine the optimal range of transmembrane gas pressure in an MABR system for cost-efficient nitrogen removal from ammonium-rich wastewaters on basis of oxygen profile analysis.

Materials and methods

Reactor configuration

The MABR used in this study is shown in Fig. 1. This reactor, which houses a membrane module, had a working volume of 6.8 L including the recirculation line and was completely mixed because of its high recirculation rates. The membrane module consisted of 24 tubes of gas-permeable poly(dimethylsiloxane) (PDMS) membrane (Shanghai Yiyan Rubber Products Co. Ltd.) as the substratum for biofilm growth. The length of each tube is 440 mm. The inner and outer diameters of the silicone tube were 2.0 and 3.0 mm, respectively. The flow rate in recirculation loop of the MABR system was monitored by a flowmeter and was stably controlled at about 250 L h^{-1}, which indicated the flow velocity above biofilm surface was about 0.014 m s^{-1}. Oxygen was supplied from the silicone membrane to the biofilm, while ammonium was provided through the liquid phase. The membrane surface area available for biofilm attachment and oxygenation in the MABR was 0.12 m^2. Pressured, filtered air was used as the gas source to supply oxygen to the system. The gas pressures used in this study were 2, 5, 10, 12, 15, 18, and 20 kPa. No significant expansion of the silicone tube was observed in this range of gas pressure (2–20 kPa). The temperature of air and water supplied to the system was kept at 27 ± 1 °C.

Medium

The MABR was fed synthetic wastewater with a peristaltic pump (Ismatech. MV-MS/CA8C, Glattburg, Zürich, Switzerland). The influent was prepared with deionized water

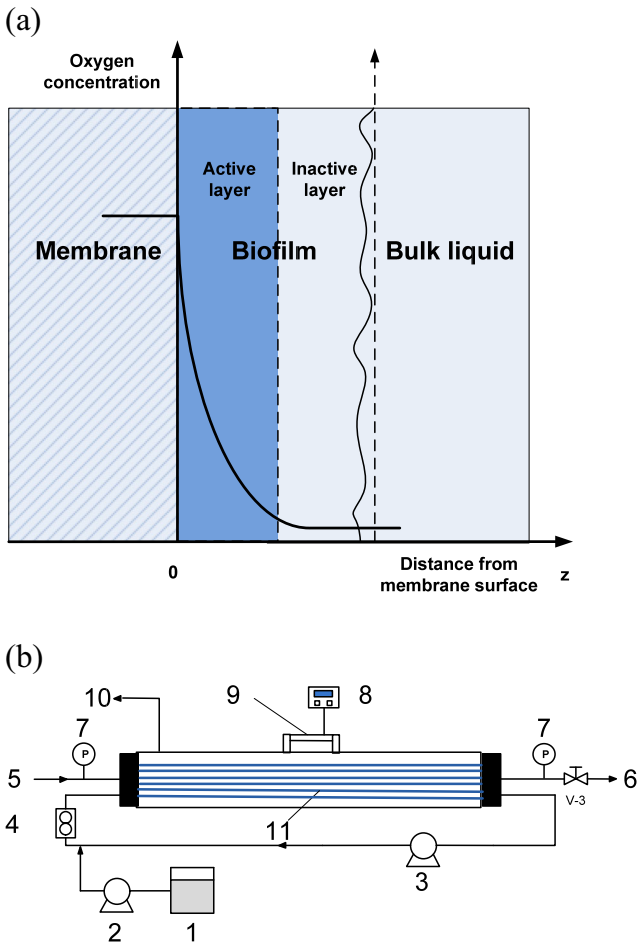

Fig. 1 Schematic of oxygen profile in membrane-aerated biofilm (**a**) and its reactor system (**b**): *1*, feed tank; *2*, influent; *3*, recirculation pump; *4*, flowmeter; *5*, aeration; *6*, air outlet; *7*, pressure gage; *8*, DO/pH meter; *9*, port for microelectrode; *10*, effluent; *11*, silicone membrane

and contained NH_4HCO_3 (N source) and $NaHCO_3$ (C source and buffer). The influent $NaHCO_3$ concentration varied depending on the required buffer capacity, while the influent ammonium concentration and flow rate were adjusted to obtain the desired N load and hydraulic retention time (HRT). In addition, the feed contained 0.02 g of phosphorus (P) L^{-1} and 1 mL L^{-1} of a trace element solution after Pynaert et al. (2004) and had a pH of 7.5–8.3.

Inoculation and start-up

The system was inoculated with activated sludge from a lab-scale nitrifying reactor. After inoculation, the system was operated in batch mode until ammonia removal could be detected. Then, the operation was switched to continuous influent mode. The first day of continuous mode operation was recorded as the first day of operation time (day 1). During the process of biofilm development, from day 1 to day 98, the transmembrane gas pressure was set at 2 kPa; after the biofilm was mature, the transmembrane gas pressure was changed, from 2 to 20 kPa, from day 99 to day 122. The biofilm thickness was double-checked at approximately 600 ± 12 μm during this period of time. Compared to the variation in reaction and diffusion in this biofilm, which occurred on a much shorter timescale, the change in biofilm thickness was negligible in this study.

Chemical analysis

The concentrations of NH_4^+-N, NO_2^--N, and NO_3^--N were measured by a spectrophotometer (UV-1800, Shimadzu, Japan) following the procedures of standard methods (APHA, 2005). Oxygen microsensor measurements in the biofilm were conducted with a 10-μm Clark-type oxygen microsensor (OX10, Unisense A/S). The sensor was inserted directly into the biofilm from the bulk liquid through a small hole in the reactor lid for in situ profiling using the Unisense MicroProfiling System. The sensor was moved from the bulk liquid into the biofilm at intervals of 5 μm with a motor-driven motor controller (Model MC-232, Unisense A/S) and a micromanipulator (Model MM33-2, Unisense A/S).

Positioning the membrane and biofilm surfaces

Since the fluxes of oxygen and ammonia are determined at the membrane surface and the biofilm surface, respectively, positioning these surfaces on the oxygen profiles is important. The membrane/biofilm interface can be located by using DO profiles of the biofilm measured via an oxygen microelectrode. Figure 1a shows a schematic of the oxygen profile of the membrane-aerated biofilm. When the tip of microelectrode penetrated the entire biofilm and touched the silicone membrane, the oxygen profile demonstrated an obvious change from curve to straight line (see Fig. 4); this inflection point was used to locate the surface of the membrane.

While an oxygen microelectrode was used to measure the DO profiles in the biofilm, a stereomicroscope (Szm0745T, Gamry Optical Instrument Co. Ltd., Ningbo, China) was used to observe the whole measurement site. Once the tip of the electrode attached to the surface of the biofilm in the view of the computer connected to the stereomicroscope, there was a small turning point and then the depth and signal were recorded so as to position the surface of the biofilm. The biofilm thickness is defined as the distance between membrane/biofilm interface and biofilm surface. The oxygen penetration depth (d_p) is defined as the depth in the biofilm where DO concentration is approximately 0.1 mg L^{-1}. We conducted DO profile measurements in at least three replications per assay.

Conceptual demonstration of oxygen transfer in membrane-aerated biofilm at different transmembrane gas pressure was presented in two-dimensional graphs with the assumption that DO distribution along the membrane was uniform. The distance long the membrane was set as

1000 μm and the distance from membrane surface was set as 700 μm. DO concentration gradients and DO penetration depth were illustrated in the two-dimensional graphs, which visualized the oxygen transfer in membrane-aerated biofilms at different P_g.

Oxygen concentration gradient and oxygen flux

According to Fick's first law, an oxygen concentration gradient (dS_{O2}/dz) is the driving force for the one-dimensional diffusion of oxygen in biofilm, and the oxygen flux (J_{O2}) is calculated as follows:

$$J_{O2} = -D_{eff}\frac{dS_{O2}}{dz} \quad (1)$$

where D_{eff} is the effective diffusion coefficient of oxygen in biofilm (m^2 day^{-1}), S_{O2} is the oxygen concentration (g m^{-3}), and z is the depth dimension normal to the membrane surface. Since the oxygen concentration always decreases from the membrane surface to the biofilm surface, the value of oxygen gradient (dS_{O2}/dz) is always negative in membrane-aerated biofilms, which gives a positive oxygen flux from membrane to biofilm surface. The density of autotrophic nitrifying biofilm used in this study is relatively high compared to that of a heterotrophic biofilm; therefore, D_{eff} is considered to be half of D_w for dense biofilm (Horn and Morgenroth, 2006). A D_w of 2.2×10^{-4} m^2 day^{-1} was used for the oxygen diffusion coefficient in water (Thibodeaux, 1979), so D_{eff} is 1.1×10^{-4} m^2 day^{-1} in this study.

The oxygen concentration (S_{O2}) in biofilm is influenced by reaction and diffusion. In nitrifying biofilms, the oxygen flux (J_{O2}) can be divided into two parts: (1) an oxygen flux utilized by nitrifying bacteria to oxidize ammonium ($J_{O2,\ reaction}$) and (2) an oxygen flux utilized by other processes (such as endogenous respiration) and diffusion ($J_{O2,\ other}$).

$$J_{O2} = J_{O2,reaction} + J_{O2,other} \quad (2)$$

where J_{O2} is the total oxygen flux entering biofilm (g m^{-2} day^{-1}), $J_{O2,\ reaction}$ is the oxygen flux utilized by biological ammonium oxidization (g m^{-2} day^{-1}), and $J_{O2,\ other}$ is the oxygen flux utilized by other processes and diffusion (g m^{-2} day^{-1}).

Statistical analysis

All assays were conducted in triplicate, and the results are expressed as mean ± standard deviation. An analysis of variance (ANOVA) was used via SPSS Statistics 17.0 to test the significance of the results, and $p < 0.05$ was considered to be statistically significant.

Results

Specific ammonium removal rate

A bench-scale MABR with a relatively fixed biofilm thickness (600 ± 12 μm) was operated at a variety of transmembrane pressures (P_g) to determine the effect of P_g on nitrogen transformation performance in the MABR, and the results are presented in Fig. 2a. We demonstrate that when P_g increased from 2 to 10 kPa, the ammonium removal efficiency of the MABR presented a significant improvement, from 50.2 to 85.5 %. However, when P_g increased from 10 to 20 kPa, the average ammonium removal efficiency increased just slightly, from 85.5 to 90.3 %. It can be concluded that in a certain range of gas pressure (2–10 kPa in this study), the ammonium removal in an MABR can be enhanced by increasing P_g but that when P_g exceeds this range, the ammonium removal efficiency cannot be improved proportionally with an increase in P_g. Therefore, a threshold in transmembrane gas pressure, or P_g^t, exists for ammonium removal in an MABR. The threshold value of transmembrane gas pressure for ammonium removal in an MABR is defined as the value of P_g that ammonium removal cannot be further improved significantly when transmembrane gas pressure goes beyond this value. P_g^t was determined to be 10 kPa in this study. Because of the higher energy consumption required to raise a P_g over P_g^t, P_g^t is identified as the optimal P_g for ammonium removal in an MABR in terms of the energy consumption of maintaining P_g.

The variation of nitrite and nitrate concentration with P_g in an MABR is presented in Fig. 2b. When P_g increased from 2 to 5 kPa, the average effluent nitrite concentration increased from 2.8 to 7.4 mg L^{-1} and the average effluent nitrate concentration increased from 39.4 to 48.1 mg L^{-1}. When the gas pressure increased from 5 to 20 kPa, the effluent nitrate concentration increased to 68.2 mg L^{-1}, while the effluent nitrite concentration decreased to less than 2.2 mg L^{-1}. These results indicate that a limited oxygen supply causes the accumulation of nitrite, or partial nitrification, in membrane-aerated biofilm but an excessive oxygen supply results in full nitrification in an MABR.

The specific ammonium removal rate (v) increased from 4.98 to 8.78 gN m^{-2} day^{-1} when P_g increased from 2 to 10 kPa (Fig. 3). However, the specific ammonium removal rate increased only slightly from 8.78 to 9.26 gN m^{-2} day^{-1}, as P_g increased from 10 to 20 kPa.

The relationship between specific ammonium removal rate (v) and transmembrane gas pressure (P_g) is described in Eq. (3):

$$v = v_0 + \frac{v_{max} \cdot P_g}{K_p + P_g} \quad (3)$$

where v and v_{max} refer to the specific ammonium removal rate and the maximum specific ammonium removal rate,

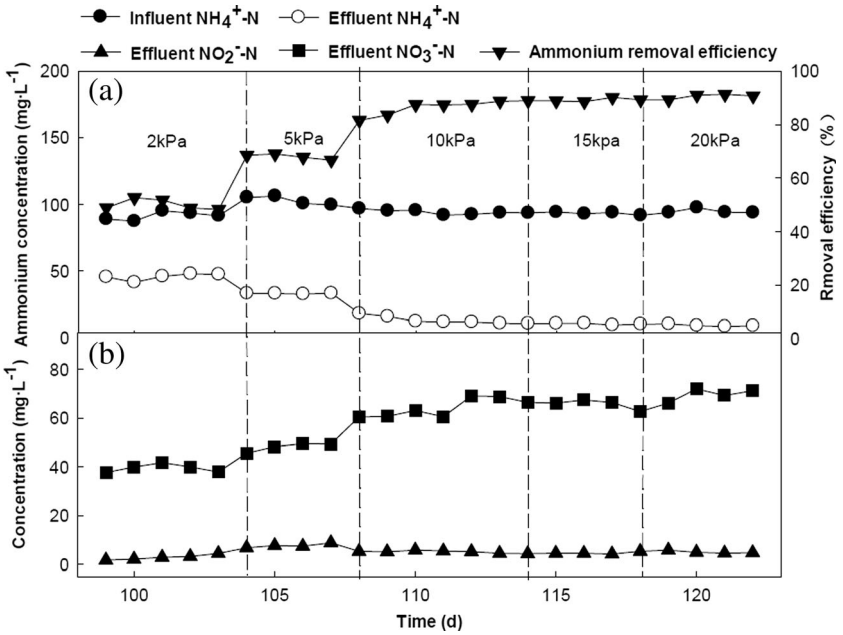

Fig. 2 Nitrogen transformation in membrane-aerated biofilm reactor at different intra-membrane gas pressure (P_g). **a** Ammonium removal, **b** nitrite and nitrate accumulation

representatively (gN m^{-2} day^{-1}); v_0 refers to the specific ammonium removal rate under 0 kPa (gN m^{-2} day^{-1}); P_g refers to the transmembrane gas pressure (kPa); and K_p refers to the coefficient of transmembrane gas pressure (kPa). Equation (3) is applicable to describing the ammonium removal performance in membrane-aerated biofilm with (1) fixed biofilm thickness and biofilm composition, (2) constant temperatures of both gas and liquid, and (3) stable hydrodynamic conditions surrounding the biofilm.

The data in Fig. 3 were regressed using Eq. (3) ($R^2 = 0.983$, $P = 0.017 < 0.05$). The constants used in Eq. (3) were calculated as follows: $v_{max} = 9.27$ gN m^{-2} day^{-1}, $K_p = 3.50$ kPa, and v_0=1.55 gN m^{-2} day^{-1}. Therefore, Eq. (3) can be rewritten as Eq. (4), which describes the relationship between the specific ammonium removal rate (v) and the transmembrane gas pressure (P_g) in the MABR in this study.

$$v = 1.55 + \frac{9.27 \cdot P_g}{3.50 + P_g} \qquad \left(R^2 = 0.983, P = 0.017 < 0.05\right) \quad (4)$$

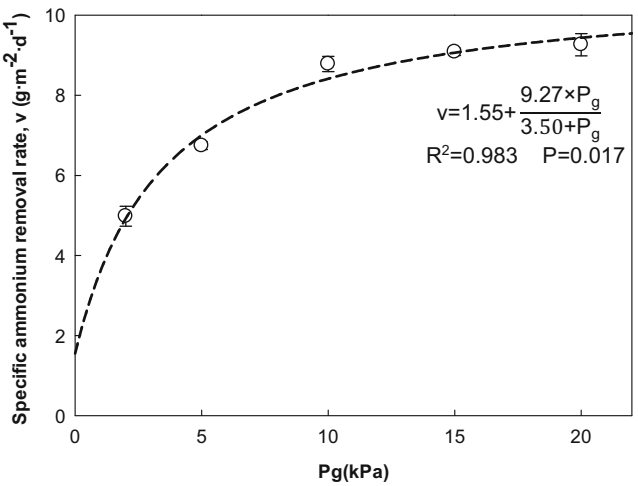

Fig. 3 Specific ammonium removal rate in membrane-aerated biofilm reactor at different intra-membrane gas pressure (P_g)

Dissolved oxygen profiles in membrane-aerated biofilm

DO profiles in the mature biofilm were directly measured under in situ conditions at different P_g from 2 to 20 kPa (Fig. 4). The DO concentration was highest at the membrane surface during all the measurements, indicating that oxygen diffused through the membrane and that DO decreased from the membrane surface to the bulk liquid.

The membrane-aerated biofilm can be divided into two layers: an active layer and an inactive layer. The active layer is near the membrane/biofilm interface, where ammonium is oxidized and oxygen is reduced. The DO profile in the active layer is a sharply decreasing curve from the membrane surface to the interface between the active layer and the inactive layer. The inactive layer is near the biofilm/bulk liquid interface, where no oxygen is consumed. The DO profile in the inactive layer is a straight line from the interface between the active layer and the inactive layer to the biofilm surface.

In order to investigate the effect of the reaction, i.e., oxygen consumption by nitrifiers to oxidize ammonium, on DO profiles in membrane-aerated biofilm, the MABR system was operated with synthetic wastewater without ammonium for 6 h and DO profiles were measured in the biofilm when no ammonium could be detected in the effluent. The DO profiles in membrane-aerated biofilm with and without ammonium in

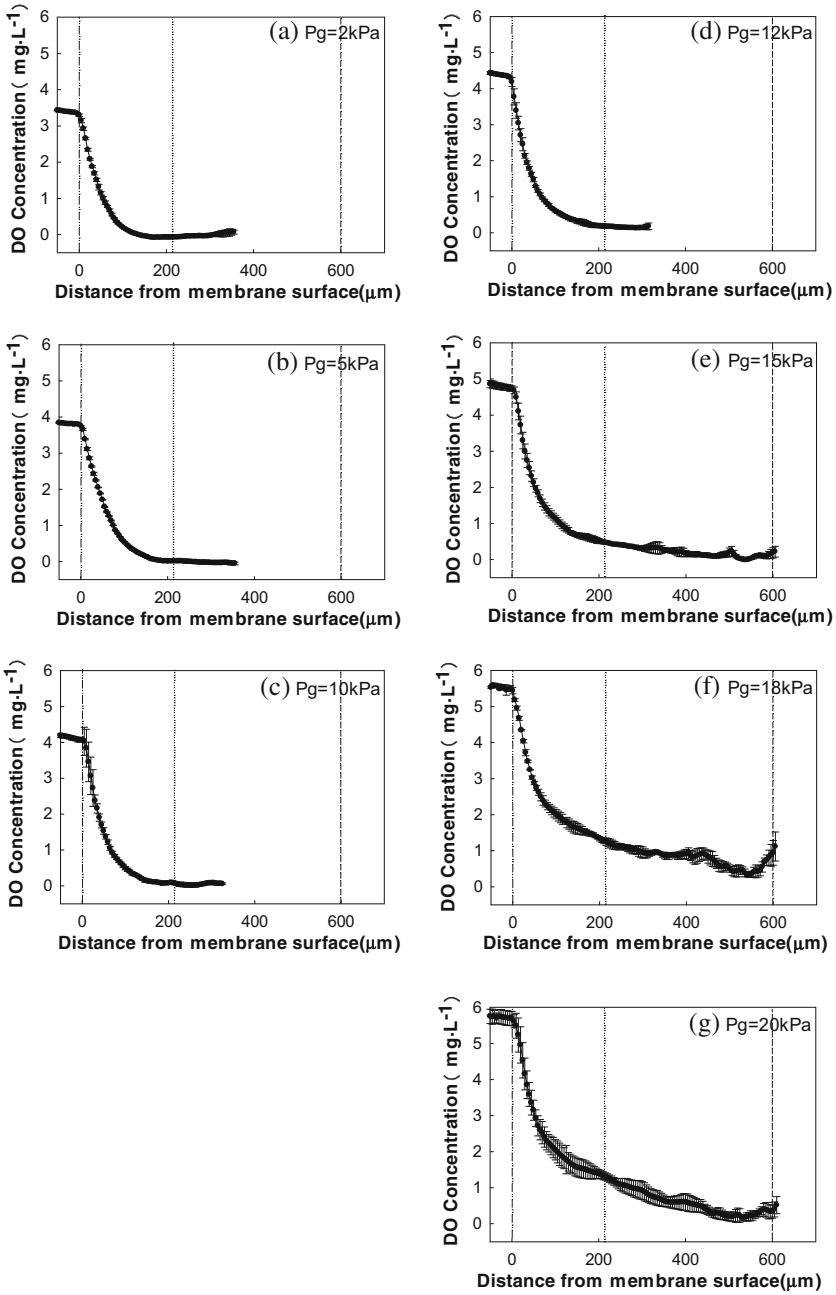

Fig. 4 DO profiles in membrane-aerated biofilm at different intra-membrane gas pressures (P_g): **a** 2, **b** 5, **c** 10, **d** 12, **e** 15, **f** 18, and **g** 20 kPa. *Dot dash line* indicates membrane surface, *dotted line* indicates interface of active and inactive layers, and *dash line* indicates biofilm surface

the influent under 15 kPa are presented in Fig. 5. Here, we demonstrate that the DO profile under 15 kPa without ammonium in the influent was almost linear, indicating almost no reaction in the biofilm and that the oxygen only penetrated from the membrane to the biofilm and bulk liquid via diffusion. The DO profile in biofilm with ammonium in the influent first had a concave down curve from the membrane surface to the point of 213 μm (the interface of the active layer and the inactive layer), which implies that the ammonium oxidization reaction occurred in this part of biofilm, i.e., the active layer. The DO profile in the inactive layer (from 213 to 600 μm) with ammonium in the influent was almost linear and parallel with the corresponding part of the DO profile without ammonium in the influent, indicating that no reaction occurred in the inactive layer whether ammonium was supplied in the influent or not.

Oxygen penetration depth

As shown in Fig. 4, different oxygen penetration depth (d_p) values were measured at various P_g (2–20 kPa; Fig. 4a–g) in the membrane-aerated biofilm. For example, d_p was shown to be lowest (=112 μm) when P_g = 2 kPa and generally increased with higher P_g values. When

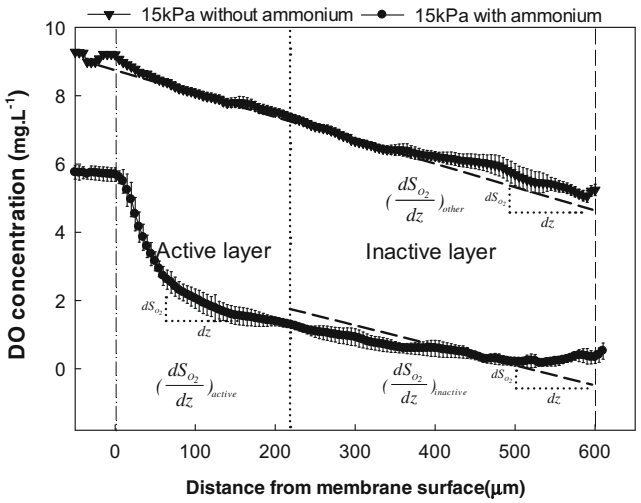

Fig. 5 DO profiles in membrane-aerated biofilm at P_g of 15 kPa with (*down-pointing triangle*) and without (*black circle*) ammonium in influent. *Dot dash line* indicates membrane surface, *dotted line* indicates the interface between active and inactive layers, and *dash line* indicates biofilm surface

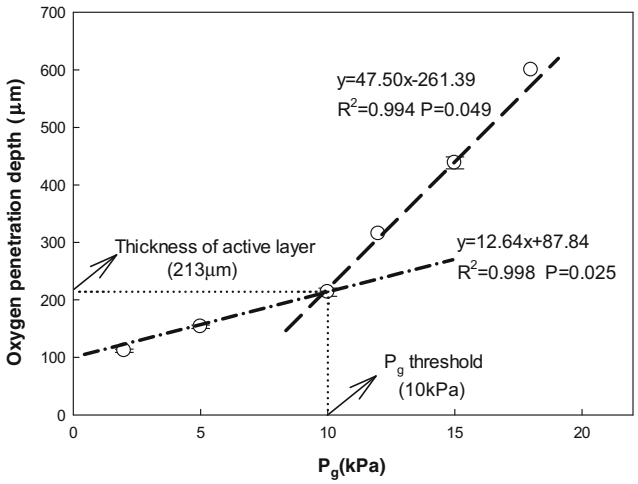

Fig. 6 Oxygen penetration depth (d_p) in membrane-aerated biofilm at different intra-membrane gas pressures (P_g)

P_g = 18 kPa and P_g = 20 kPa, dissolved oxygen penetrated the entire biofilm, as shown in Fig. 4(f–g) and d_p = 600 μm.

The threshold of transmembrane gas pressure, P_g^t, was determined to be 10 kPa in this study. It can be seen that when P_g is smaller than P_g^t (10 kPa), oxygen partially penetrates the active layer and is used up completely; when P_g equals P_g^t (10 kPa), oxygen penetrates the entire active layer and is used up entirely; and when P_g exceeds P_g^t (10 kPa), oxygen penetrates the inactive layer and then diffuses into the bulk liquid.

When the pressure increased from 2 to 10 kPa, d_p increased from 112 to 213 μm (Fig. 6). This relationship between d_p and P_g can be described by a linear regression, Eq. (5); $R^2 = 0.998$, $P = 0.025$.

$$d_p = 12.64 \times P_g + 87.84 \qquad (R^2 = 0.998, P = 0.025) \tag{5}$$

When the pressure increased from 12 to 18 kPa, d_p increased sharply from 315 to 600 μm. The linear regression is presented as Eq. (6); $R^2 = 0.994$, $P = 0.049$.

$$d_p = 47.50 \times P_g - 261.4 \qquad (R^2 = 0.994, P = 0.049) \tag{6}$$

The slopes of the regressed lines in Fig. 6 represent the ratio of d_p to P_g. When P_g changed from 2 to 10 kPa, d_p did not exceed the active layer (213 μm), and the slope of the regressed line is 12.64 μm kPa^{-1}. When P_g changed from 10 to 20 kPa, d_p exceeded the active layer (213 μm), and the slope of the regressed line is 47.50 μm kPa^{-1}. Therefore, it can be concluded that the ratios of d_p to P_g in the active layer and the inactive layer are both constant; however, the ratio of d_p to P_g in the active layer is significantly smaller than that in the inactive layer.

These experimental results demonstrate that the biofilm was composed of an active and an inactive layer and that the thickness of the active layer can be determined from the d_p where the slope of d_p over P_g changed. The position of the P_g threshold coincides with the thickness of the active layer, as shown in Fig. 6, so the thickness of the active layer in a MAB (213 μm in this study) can be determined on the basis of the change in the slope of d_p over P_g.

Ratios of d_p to P_g are affected by biofilm activity and oxygen diffusivity. The variation in DO concentration in the active layer reflects two processes: one is oxygen diffusion from the membrane surface to the biofilm surface and the other is oxygen consumption by the active bacteria for ammonium oxidization. The combination of oxygen diffusion and oxygen consumption results in a concave down curve (see Fig. 4) in DO profiles. However, there was almost no reaction in the inactive layer: oxygen could only penetrate the biofilm by diffusion, so d_p increased more quickly in the inactive layer than in the active layer.

As P_g went from 2 to 10 kPa, d_p did not exceed the active layer (213 μm) and nitrifiers in the active layer were able to get enough oxygen to oxidize ammonium. When the pressure increased to 20 kPa, d_p exceeded the active layer and oxygen penetrated the inactive layer. Since there was almost no reaction in the inactive layer, the ammonium removal cannot be further improved significantly. This result is consistent with those showing that the highest specific ammonium removal rate (v) is achieved when P_g equals P_g^t (10 kPa) and that v

cannot be improved significantly when P_g exceed P_g^t (see Fig. 3).

Oxygen concentration gradient and utilization

A series of experiments was conducted to measure the oxygen profiles in biofilm without ammonium oxidization. A linear concentration profile was observed all through the biofilm, from the membrane surface to the biofilm surface, which indicates that the oxygen concentration was controlled by diffusion alone and that there was negligible reaction or endogenous respiration occurring in the entire biofilm without ammonium feeding. The oxygen flux without reaction ($J_{O2,\ other}$) can be calculated from the slope of the linear oxygen concentration profile without ammonium feeding, $\left(\frac{dS_{O2}}{dz}\right)_{other}$.

$$J_{O2,other} = -D_{eff}\left(\frac{dS_{O2}}{dz}\right)_{other} \quad (7)$$

When the oxygen profiles in biofilm with (black circle) and without (down-pointing black triangle) ammonium feeding are put together in the same graph (Fig. 5), it can be seen that the oxygen profile with ammonium feeding is curved when reaction and diffusion occurred simultaneously in the active layer of the biofilm, from the membrane surface ($z = 0$ μm) to the boundary of the active layer ($z = 213$ μm). It can also be seen that the profile with ammonium feeding is linear in the inactive layer of the biofilm, from the boundary of the active layer ($z = 213$ μm) to the biofilm surface, while the corresponding profile in the biofilm without ammonium feeding is parallel to the linear concentration. The parallelism between the two profiles makes it possible to calculate the oxygen flux without reaction ($J_{O2,\ other}$) based on the oxygen concentration gradients in the inactive layer of the membrane-aerated biofilm, $\left(\frac{dS_{O2}}{dz}\right)_{inactive}$.

$$J_{O2,other} = -D_{eff}\left(\frac{dS_{O2}}{dz}\right)_{other} = -D_{eff}\left(\frac{dS_{O2}}{dz}\right)_{inactive} \quad (8)$$

We combine Eqs. 6 and 8 to obtain the oxygen flux utilized for the reaction ($J_{O2,\ reaction}$).

$$J_{O2,reaction} = J_{O2} - J_{O2,other} = -D_{eff}\left(\frac{dS_{O2}}{dz}\right)_{active} + D_{eff}\left(\frac{dS_{O2}}{dz}\right)_{inactive} \quad (9)$$

where $\left(\frac{dS_{O2}}{dz}\right)_{active}$ is the oxygen concentration gradient in the active layer of the membrane-aerated biofilm (Fig. 5).

The oxygen flux utilized for the reaction ($J_{O2,\ reaction}$) equals the oxygen utilization rate for ammonium oxidization, which reflects the local activity of nitrifiers in the biofilm. The oxygen utilization activities for ammonium oxidization in membrane-aerated biofilm at various P_g were calculated from Eq. 9 (Fig. 7). In all cases, there is a narrow peak for oxygen utilization activities within the range of about 30 μm from the membrane surface. The existence of an activity peak in the middle of a counter-diffusion biofilm is reasonable, as it is the location in the biofilm where both ammonium and oxygen are present. At the base of the biofilm, the oxygen concentration is high but ammonium is limited; in contrast, at the top of the biofilm, ammonium is plentiful but the oxygen has been almost used up.

The maximum oxygen utilization activities in membrane-aerated biofilm at various P_g are shown in Fig. 8. The data were regressed with the Gaussian process regression method, and the regressed curve ($R^2 = 0.6853$,$P = 0.2696$) is presented as a dashed line in Fig. 8. It is obvious that the highest oxygen utilization activity was reached when P_g was 10 kPa. Higher P_g did not result in higher activity in nitrifying biofilm. The reason for this result needs further investigation.

Discussion

Oxygen concentration on the membrane surface

Based on the DO profiles in biofilms at various P_g (Fig. 4), we observed that DO concentrations at the membrane surface ($S_{O2,m}$) varied from 3.3 mg L^{-1} at a P_g of 2 kPa to 5.7 mg L^{-1} at a P_g of 20 kPa, with $S_{O2,m}$ positively correlating with P_g (Fig. 9). A linear regression was conducted, and Eq. (10) was obtained to show the relationship between $S_{O2,m}$ and P_g with $R^2 = 0.950$ and $P = 0.0002$.

$$S_{O2,m} = 0.130 + 2.941 \times P_g \qquad (R^2 = 0.950, P = 0.0002) \quad (10)$$

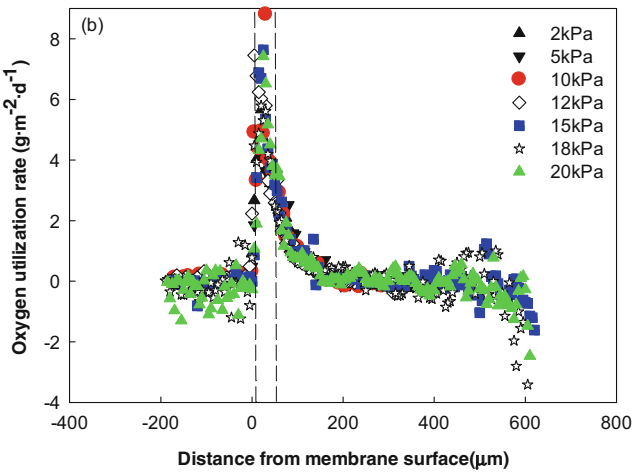

Fig. 7 Oxygen utilization rate in membrane-aerated biofilm at different intra-membrane gas pressure (P_g)

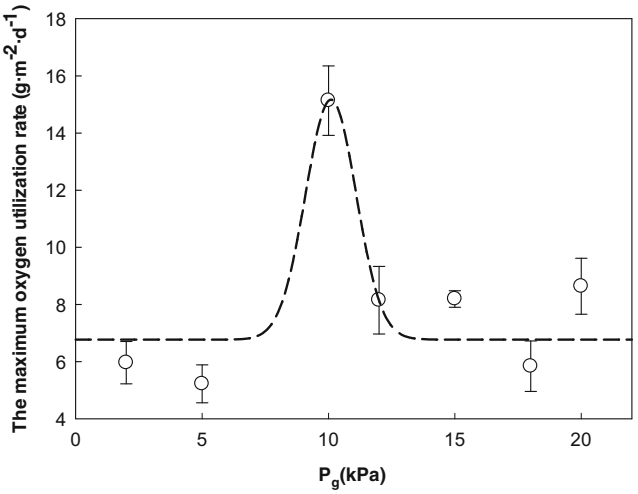

Fig. 8 Maximum oxygen utilization rate in active layer of membrane-aerated biofilm at different intra-membrane gas pressure (P_g)

where $S_{O2,m}$ refers to the DO concentration at the membrane surface (mg L^{-1}) and P_g refers to the transmembrane gas pressure (kPa). It has also been reported in the literature (Terada et al., 2006; Downing and Nerenberg, 2008) that the measured DO concentration at the membrane surface can be less than that predicted by Henry's Law, possibly because of the decreased oxygen transfer at lower transmembrane pressures. The values of $S_{O2,m}$ reported by Downing and Nerenberg (2008) varied from 2.2 to 5.5 mg L^{-1} when P_g increased from 14 to 70 kPa; these values are in the same range as the results reported here. However, the results in this study are lower than those reported by Lackner et al. (2010), who observed that the oxygen concentration at the membrane surface increased from 5.6 mg L^{-1} (at 0 kPa) to 8.6 mg L^{-1} (at 5 kPa). In addition, Satoh et al. (2004) demonstrated that a higher P_g did not necessarily result in a higher oxygen concentration at the membrane surface. This incongruence between study results may be related to membrane material and the range of oxygen pressure.

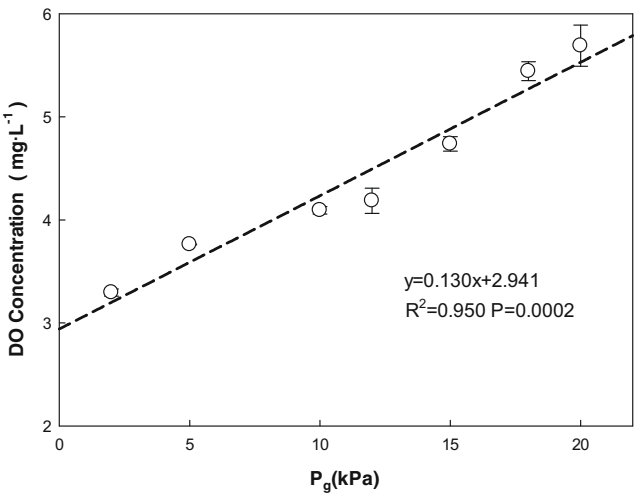

Fig. 9 DO concentration at the membrane surface at different intra-membrane gas pressure (P_g)

Higher oxygen concentration on the membrane surface provides a higher drive force for oxygen penetration in biofilm and results in a higher oxygen penetration depth. However, the relationship between oxygen concentration on the membrane surface and ammonium removal rate is not linear. When oxygen penetration depth is below the thickness of active layer in biofilm, the ammonium removal rate increased with the increase of P_g and $S_{O2,m}$. But the ammonium removal rate cannot be improved linearly with the increase of P_g and $S_{O2,m}$ when oxygen penetration depth exceeds the thickness of active layer in biofilm.

Interactions between oxygen diffusion and the active layer

A mature nitrifying membrane-aerated biofilm is composed of two layers, an ammonia-oxidizing active layer near the membrane surface and an ammonia-oxidizing inactive layer away from the membrane; see Fig. 1. The mature biofilm indicates the biofilm which is fully developed and has adequate biofilm thickness and stratified structure. Generally, a mature nitrifying biofilm is higher than 200 μm based on the observation in our experiments.

Oxygen can diffuse through the gas phase to the membrane surface and then penetrate the biofilm. Because of the mass transfer resistance and oxygen consumption during ammonium oxidization in the biofilm, the oxygen concentration is the highest at the membrane surface and decreases along the biofilm thickness from the membrane surface. Satoh et al. (2004) observed that the transmembrane air pressure had no effect on the location of the nitrification and denitrification zones. The thickness of the active layer was not dependent on P_g in this study either, remaining almost constant at about 213 μm under various P_g, and the inactive layer was located from 213 to 600 μm from the membrane surface (Fig. 10).

In this study, the optimal conditions for ammonium removal were met when the transmembrane gas pressure was 10 kPa, the DO concentration at the membrane surface was approximately 4.1 mg L^{-1} with the bulk liquid anoxic, and the oxygen penetration depth was approximately 213 μm. These results suggest that there is a threshold transmembrane gas pressure (P_g^t) for ammonium removal and that the position of this threshold is related to the oxygen penetration depth (d_p) in the biofilm. When P_g increased from 2 to 10 kPa, d_p had not exceeded the interface of the active layer and the inactive layer, conceptually shown in Fig. 10 (a–c). The nitrifiers in the active layer obtained adequate oxygen to oxidize ammonium into nitrite and nitrate, and they consumed oxygen as fast as possible. This caused the specific ammonium removal rate to increase sharply from 4.98 to 8.78 gN m^{-2} day^{-1}. When P_g increased beyond the threshold, from 10 to 12 and even to 20 kPa, the oxygen diffused into the inactive layer, which resulted in a rapid increase in d_p, as shown in Fig. 10(d–g). Since the microorganism activity in the inactive layer was much weaker than that in the active layer, the oxygen consumption by

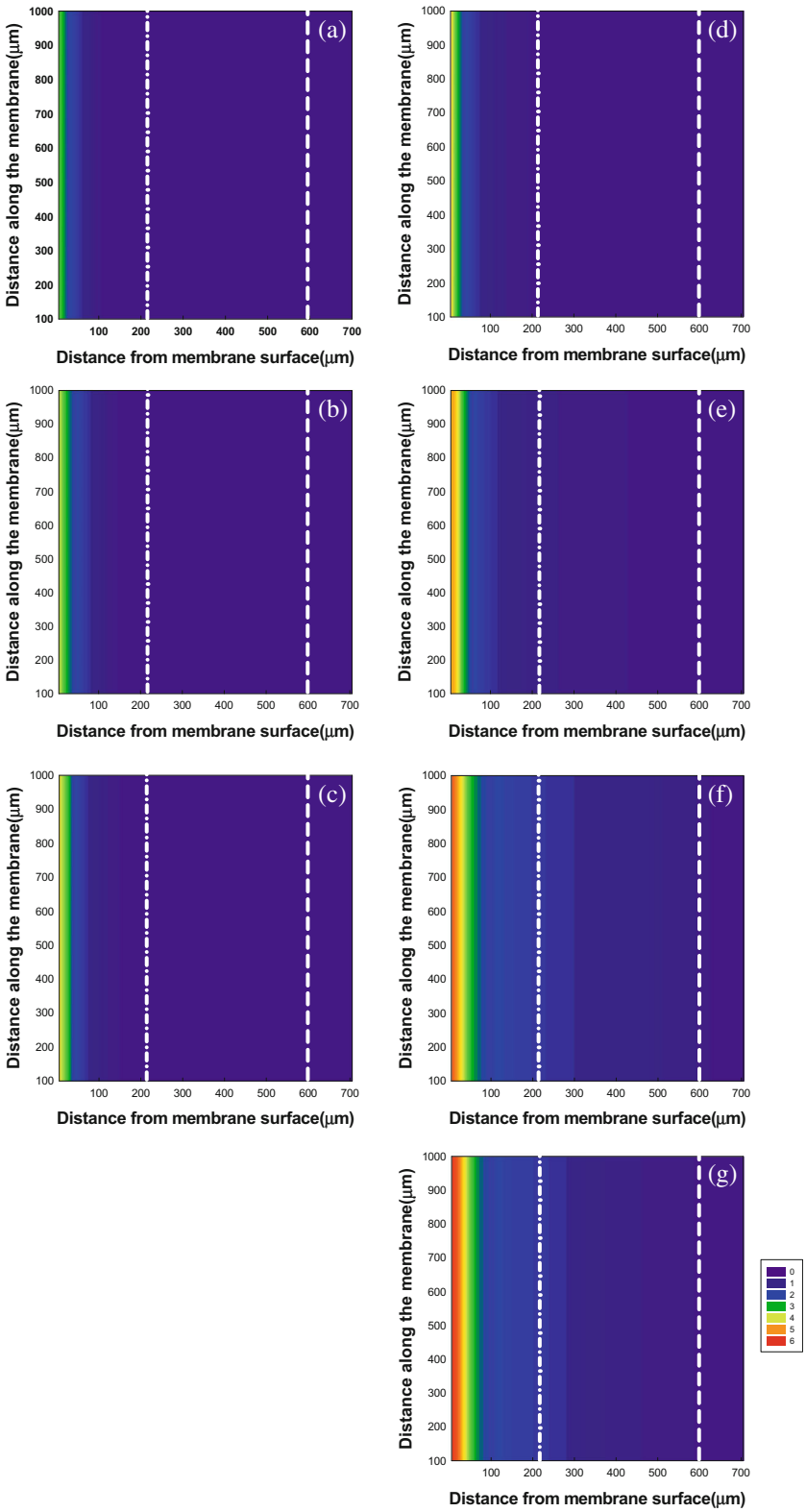

Fig. 10 Conceptual demonstration of oxygen transfer in membrane-aerated biofilm at different intra-membrane gas pressures (P_g): **a** 2, **b** 5, **c** 10, **d** 12, **e** 15, **f** 18, and **g** 20 kPa. *Dot dash line* indicates the interface between active and inactive layers; *dash line* indicates biofilm surface. It is assumed that DO distribution along the membrane is uniform

microorganisms in the inactive layer was consequently much lower, which in turn led to deeper oxygen penetration in the biofilm; however, the ammonium removal rate did not increase obviously.

Shanahan and Semmens (2004) reported that the peak activity of nitrifiers occurred in counter-diffusion biofilm using a multipopulation model, but they predicted that nitrifiers operated at their highest activities about 180 μm from the membrane

surface in a biofilm 800 μm thick. It was also reported by other researchers (Downing and Nerenberg, 2008; Lackner, et al., 2010) and confirmed by our previous work (Wang, et al., 2009; Wang, et al., 2011) that most of the nitrifying bacteria were in the region adjacent to the membrane surface.

The changes of oxygen penetration depths at different P_g presented here are slightly different from those reported by Lackner et al. (2010), who used microelectrodes to measure oxygen profiles in counter-diffusion biofilm at various gas pressures (0, 1.0, and 5.0 kPa) and observed that the oxygen penetration depth was approximately 125 μm in all profiles with a biofilm thickness estimated between 650 and 800 μm. We observed that the oxygen penetration depth increased as the transmembrane gas pressure increased. The reason for the difference may be that different ranges of gas pressure were applied in these two studies. The range of gas pressure reported by Lackner et al. (2010) is from 0 to 5 kPa, which is much lower and narrower than the range of gas pressure applied in this study, which is from 2 to 20 kPa. The variation of d_p may have been too slight to be observed when a narrow range of low pressure was applied. The inconformity in d_p may also be attributed to the difference of gas-permeable membrane material, membrane thickness, and lateral flow velocities applied in these two studies.

Implications for MABR applications

Satoh et al. (2004) reported that the transmembrane air pressure had no effect on the start-up or the maximum rates of nitrification in MABRs at a low COD loading rate. Downing and Nerenberg (2008) observed that the ammonium flux decreased with a decrease in P_g, most likely because of an increasing oxygen limitation in the biofilm. Zhu et al. (2009) found that a higher oxygen flux resulted in a less stable biofilm, and there existed a critical oxygen partial pressure for sustaining a membrane-aerated biofilm at a given COD load. However, in this study, no organic carbon was fed in the MABR system, and according to the results, we can conclude that there is a threshold of transmembrane gas pressure for ammonium removal in an MABR. Beyond this threshold, ammonium removal cannot be improved dramatically.

The threshold of P_g for ammonium removal in an MABR is useful for guiding the design of MABR systems for treating various wastewaters, especially those rich in ammonia. Applying a higher gas pressure in an MABR always means higher costs of energy and operation. However, we have shown a higher gas pressure and/or higher oxygen flux does not necessarily result in a higher ammonium removal efficiency when a relatively fixed active nitrifying biomass is available in the reactor system.

On the other hand, higher gas pressure does not necessarily result in high gas transfer flux. An apparent decrease in oxygen mass transfer coefficient at higher oxygen pressure was attributed to the formation of micro-bubbles on the membrane surface (Cote et al., 1989). If oxygen transfers from membrane to bulk liquid and cannot be removed from membrane surface quickly, oxygen molecules will accumulate at membrane surface and form micro-bubbles when the oxygen pressure exceeds a saturation point. However, biofilm growing on membrane surface makes the mass transfer at the membrane-biofilm interface more complex in membrane-aerated biofilm. Whether micro-bubbles form at higher intra-membrane gas pressure or not needs further investigation and confirmation.

The threshold of P_g (P_g^t) in an MABR can be different in different reactor systems. The microbial composition and structure of the nitrifying membrane-aerated biofilm will affect the value of P_g^t. For example, different species of ammonium-oxidizing bacteria have different oxygen half-saturation constants ($K_{s,\ O2}$), which affect the value of P_g^t. Moreover, the distribution of density and diffusivity in a biofilm will affect the value of P_g^t. Here, it is assumed that the density and diffusivity in the biofilm are constant and are represented by the average value. However, further investigation of the effect of local diffusivity on P_g^t needs to be conducted. In addition, the material, composition, and surface characteristics of a gas-permeable membrane may also influence the oxygen transport in the biofilm.

The results presented here may not be applicable for young biofilms in MABR, where oxygen can penetrate the whole biofilm and no oxygen-limiting condition exists in the whole biofilm. Generally, during the start-up stage of MABR, the membrane lumen was kept unpressurized or provided with very low pressure to avoid supersatuation conditions and bubble formation on the membrane surface that impeded bacterial attachment and biofilm development (Pellicer-Nàcher et al., 2013).

When an MABR for ammonium removal from wastewaters has been started up and a relatively stable biofilm with thickness more than 200 μm has developed on membrane surface, dissolved oxygen profiles within membrane-aerated biofilm can be collected at different P_g (e.g., from 0 to 50 kPa at intervals of 5 kPa) with the aid of oxygen microelectrode and the oxygen penetration depth (d_p) within the biofilm can be measured based the oxygen profiles. Two straight lines can be regressed on the plot of d_p vs. P_g as shown in Fig. 5. The line within the active layer of biofilm has a lower slope and the line within the inactive layer has a higher slope. The value of P_g at intersection of the two lines is the threshold of P_g, i.e., P_g^t. Since the ammonium removal of the MABR cannot be improved significantly when P_g goes beyond P_g^t, the MABR is recommended to be operated at P_g no higher than P_g^t.

Further research investigating the dynamics of nitrogen transformation in membrane-aerated biofilms should consider the coupling of oxygen profiles with others, such as ammonium, nitrite, and nitrate. The focus of this study is to demonstrate the existence of an optimal

P_g threshold and the possibility of determining the thickness of the active layer from oxygen profiles alone. Graphic analysis of oxygen profiles in biofilms can be a powerful and convenient tool for manipulating membrane-aerated biofilms to achieve specific objectives, such as pollutant removal and chemical conversion or production, especially in full-scale practical applications of MABR.

The goal of this study was to investigate the effect of transmembrane gas pressure (P_g) on the ammonium removal rate in a membrane-aerated biofilm reactor (MABR). The following conclusions were reached:

1. There is a threshold for the transmembrane gas pressure (P_g^t) for ammonium removal in an MABR; i.e., the ammonium removal cannot be improved significantly by increasing P_g beyond P_g^t. For practical reasons, P_g^t is identified as the optimal P_g for ammonium removal in an MABR.
2. A mature membrane-aerated nitrifying biofilm is composed of an ammonia-oxidizing active layer and an ammonia-oxidizing inactive layer. The active layer is near the membrane/biofilm interface, where ammonium is oxidized and oxygen is reduced. The inactive layer is near the biofilm/bulk liquid interface, where no oxygen is consumed. When P_g is smaller than P_g^t, oxygen partially penetrates the active layer and is used up completely; when P_g equals P_g^t, oxygen penetrates the whole active layer and is used up entirely; and when P_g exceeds P_g^t, oxygen penetrates the inactive layer and then diffuses into bulk liquid.
3. The ratio of the oxygen penetration depth (d_p) to P_g is influenced by oxygen transfer flux and oxygen utilization rate in a nitrifying biofilm. The ratios of d_p to P_g in the active layer and the inactive layer are both constant; however, the ratio of d_p to P_g in the active layer is significantly smaller than that in the inactive layer. The thickness of the active layer can be determined from the location at which the ratio of d_p to P_g changes.

Acknowledgments This research was funded by the National Science & Technology Pillar Program in China (2012BAJ21B01), the National Natural Science Foundation of China (50908164), the Fundamental Research Funds for the Central Universities in Tongji University, and the 111 Project in Tongji University from the Programme of Introducing Talents of Discipline to Universities, MOE. The authors thank Kathryn Stewart for her help with editing the manuscript.

Compliance with ethical standards

Conflict of interest The authors declare that they have no conflict of interest.

Ethical approval This article does not contain any studies with human participants or animals performed by any of the authors.

References

APHA (2005) Standard methods for the examination of water and wastewater. American Public Health Association, Washington, DC

Brindle K, Stephenson T, Semmens MJ (1998) Nitrification and oxygen utilisation in a membrane aeration bioreactor. J Membrane Sc 144: 197–209

Casey E, Glennon B, Hamer G (2000) Biofilm development in a membrane-aerated biofilm reactor: effect of intra-membrane oxygen pressure on performance. Bioprocess Eng 23:457–465

Casey E, Rishell S, Glennon B, Hamer G (2004) Engineering aspects of a mixed methanotrophic culture in a membrane-aerated biofilm reactor. Water Sci Technol 49(11–12):255–262

Chen X, Guo J, Shi Y, Hu S, Yuan Z, Ni B (2014) Modeling of simultaneous anaerobic methane and ammonium oxidation in a membrane biofilm reactor. Environ. Sci. Technol. 48:9540–9547

Cote P, Bersillon JL, Huyard A (1989) Bubble-free aeration using membranes: mass transfer analysis. J Membrane Sci. 47:91–106

Downing LS, Nerenberg R (2008) Effect of oxygen gradients on the activity and microbial community structure of a nitrifying, membrane-aerated biofilm. Biotechnol Bioeng 101:1193–1204

Grady CPLJ, Daigger GT, Love NG, Filipe CDM (2011) Biological wastewater treatment (third edition). IWA Publishing, CRC Press, Taylor & Francis Group, London

Hibiya K, Terada A, Tsuneda S, Hirata A (2003) Simultaneous nitrification and denitrification by controlling vertical and horizontal microenvironment in a membrane-aerated biofilm reactor. J Biotechnol 100:23–32

Hwang JH, Cicek N, Oleszkiewicz J (2009) Effect of loading rate and oxygen supply on nitrification in a non-porous membrane biofilm reactor. Water Res 43:3301–3307

Horn H, Morgenroth E (2006) Transport of oxygen, sodium chloride, and sodium nitrate in biofilms. Chem Eng Sci 61:1347–1356

Kumar A, Hille-Reichel A, Horn H, Dewulf J, Lens P, Van Langenhove H (2012) Oxygen transport within the biofilm matrix of a membrane biofilm reactor treating gaseous toluene. J Chem Technol Biotechnol 87(6):751–757

Lackner S, Terada A, Horn H, Henze M, Smets BF (2010) Nitritation performance in membrane-aerated biofilm reactors differs from conventional biofilm systems. Water Res 44:6073–6084

Nerenberg R, Kawagoshi Y, Rittmann BE (2008) Microbial ecology of a perchlorate-reducing, hydrogen-based membrane biofilm reactor. Water Res 42:1151–1159

Pellicer-Nàcher C, Domingo-Félez C, Lackner S, Smets BF (2013) Microbial activity catalyzes oxygen transfer in membrane-aerated nitritating biofilm reactors. J Membr Sci 446:465–471

Pynaert K, Smets BF, Beheydt D, Verstraete W (2004) Start-up of autotrophic nitrogen removal reactors via sequential biocatalyst addition. Environ. Sci. Technol. 38:1228–1235

Rosso D, Lothman SE, Jeung MK, Pitt P, Gellner WJ, Stone AL, Howard D (2011) Oxygen transfer and uptake, nutrient removal, and energy footprint of parallel full-scale IFAS and activated sludge processes. Water Res 45:5987–5996

Satoh H, Ono H, Rulin B, Kamo J, Okabe S, Fukushi K (2004) Macroscale and microscale analyses of nitrification and denitrification in biofilms attached on membrane aerated biofilm reactors. Water Res 38:1633–1641

Shanahan JW, Semmens MJ (2004) Multipopulation model of membrane-aerated biofilms. Environ. Sci. Technol. 38:3176–3183

Shanahan JW, Semmens MJ (2006) Influence of a nitrifying biofilm on local oxygen fluxes across a micro-porous flat sheet membrane. J. Membrane Sci. 277:65–74

Sun F, Dong W, Shao M, Lv X, Li J, Peng L, Wang H (2013) Aerobic methane oxidation coupled to denitrification in a membrane biofilm reactor: treatment performance and the effect of oxygen ventilation. Bioresource Technol. 145:2–9

Syron E, Casey E (2008) Membrane-aerated biofilms for high rate biotreatment: performance appraisal, engineering principles, scale-up, and development requirements. Environ. Sci. Technol. 42(6): 1833–1844

Terada A, Hibiya K, Nagai J, Tsuneda S, Hirata A (2003) Nitrogen removal characteristics and biofilm analysis of a membrane-aerated biofilm reactor applicable to high-strength nitrogenous wastewater treatment. J Biosci Bioeng 95:170–178

Terada A, Yamamoto T, Igarashi R (2006) Feasibility of a membrane-aerated biofilm reactor to achieve controllable nitrification. Biochem Eng J 28:23–130

Terada A, Lackner S, Tsuneda S, Smets BF (2007) Redox-stratification controlled biofilm (ReSCoBi) for completely autotrophic nitrogen removal: the effect of co- versus counter-diffusion on reactor performance. Biotechnol Bioeng 97:40–51

Thibodeaux LJ (1979) Chemodynamics: environmental movement of chemicals in air, water and soil. John Wiley & Sons, New York

Wang R, Terada A, Smets BF, Henze M, Xia S, Zhao J (2009) Nitritation performance and biofilm development of co- and counter-diffusion biofilms: modeling and experimental comparison. Water Res 43: 2699–2709

Wang R, Zhan X, Zhang Y, Zhao J (2011) Nitrifying population dynamics in a redox stratified membrane biofilm reactor (RSMBR) for treating ammonium-rich wastewater. Front Environ Sci Eng 5:48–56

Wilderer PA (1995) Technology of membrane biofilm reactors operated under periodically changing process conditions. Water Sci Technol 31:173–183

Zhu IX, Allen DG, Liss SN (2009) Effect of oxygen partial pressure and chemical oxygen demand loading on the biofilm properties in membrane-aerated bioreactors. Water Environ Res 81:289–297

Zhao HP, Ontiveros-Valencia A, Tang Y, Kim BO, Van Ginkel S, Friese D, Overstreet R, Smith J, Evans P, Krajmalnik-Brown R, Rittmann B (2014) Removal of multiple electron acceptors by pilot-scale, two-stage membrane biofilm reactors. Water Res 54:115–122